COARSENING RATES FOR A DROPLET MODEL: RIGOROUS UPPER BOUNDS

FELIX OTTO, TOBIAS RUMP AND DEJAN SLEPČEV

Abstract. Certain liquids on solid substrates form a configuration of droplets connected by a precursor layer. This configuration coarsens: The average droplet size grows while the number of droplets decreases and the characteristic distance between them increases. We study this type of coarsening behavior in a model given by an evolution equation for the film height on an n-dimensional substrate. Heuristic arguments based on the asymptotic analysis of Glasner and Witelski [6, 7] and numerical simulations suggest a statistically self-similar behavior characterized by a single exponent which determines the coarsening rate.

In this paper, we establish rigorously an upper bound on the coarsening rate in a time-averaged sense. We use the fact that the evolution is a gradient flow, i.e. a steepest descent in an energy landscape. Coarse information on the geometry of the energy landscape serves to obtain coarse information on the dynamics. This robust method was proposed in [10]. Our main analytical contribution is an interpolation inequality involving the Wasserstein distance which characterizes the coarse shape of the energy landscape. The upper bound we obtain is in agreement with heuristic arguments and numerical simulations.

1. Introduction

1.1. **Statement of the result.** Thin layers of viscous liquid are well-described by the lubrication approximation which capitalizes on the separation of horizontal and vertical length scales. It yields a single equation for the time-dependent film height $h = h(x,t) > 0$, [20]. We now introduce this equation in its non-dimensionalized form.

Let $Q \subset \mathbb{R}^n$ parametrize the substrate. We consider smooth solutions $h : (0,\infty) \times Q \to [0,\infty)$ of

$$\partial_t h - \nabla \cdot \left(M(h) \nabla \left(\frac{\partial E}{\partial h} \right) \right) \;=\; 0 \quad \text{in } (0,\infty) \times Q. \tag{1.1}$$

Here, $\frac{\partial E}{\partial h}$ denotes the L^2-gradient of the energy functional with respect to h. The total energy E is given by

$$E(h) \;=\; \int \frac{1}{2} |\nabla h|^2 + \mathcal{U}(h)\, dx, \tag{1.2}$$

where the gradient term describes the linearized contribution of the liquid-air surface energy, while $\mathcal{U}$ models the intermolecular forces between the substrate and the film, see Subsection 1.3. We shall always write $\int$ for $\int_Q$.

2000 *Mathematics Subject Classification.* 76A20, 35K55, 35Q35.

Qualitatively, the potential $\mathcal{U}$ is of the form sketched in Figure 1. We nor-

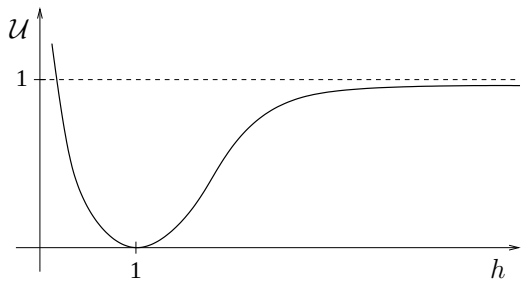

Figure 1: The intermolecular potential $\mathcal{U}$ combines repulsive and attractive forces.

malize $\mathcal{U}$ so that $\mathcal{U}(\infty) - \min \mathcal{U} = 1$ and $\operatorname{argmin} \mathcal{U} = 1$. The well-known Lennard–Jones potential [9] corresponds to $\mathcal{U}(h) = \frac{1}{3}h^{-8} - \frac{4}{3}h^{-2} + 1$ but other potentials are also physically relevant [24]. In fact, the exact expression for the potential is often not essential; as in [2, 6, 7], our results hold for a large class of potentials.

Bertozzi, Grün and Witelski [2] studied the equation (1.1) for potentials of the form $\mathcal{U}(h) = h^{-q} - h^{-p}$, $0 < p < q$ on a bounded one-dimensional substrate. If $q \geq 2$, that is if the potential blows up at zero fast enough, boundedness of the energy was used to show that solutions with positive initial data stay positive for all time. That implied that the equation has unique, classical solutions for given initial data.

In our model (1.1), we consider the linear mobility function

$$M(h) = h. \tag{1.3}$$

Let us clearly state that the appropriate mobility function for a liquid film governed by the Stokes equations with no-slip boundary condition at the substrate would be $M(h) = h^3$. In case of boundary conditions which allow a finite slip (Navier condition), the mobility would be $M(h) = h^2$ provided that film heights are small compared to the slip length, see [16, 17, 20]. The mobility function (1.3) is appropriate for a liquid film governed by the Darcy equation, as in a porous medium ($n = 2$) or a Hele–Shaw cell ($n = 1$). From the applied point of view, $M(h) = h$ is thus a rather artificial choice. It is motivated both by a technical and a conceptual consideration: The technical consideration is that only for $M(h) = h$, the induced distance in the gradient flow structure (see Appendix B) is known explicitly. The conceptual consideration is that for other mobilities, the coarse-grained slope of the energy landscape (see Section 2) overestimates the heuristically derived coarsening rates: The "collision pathways" (see Subsection 1.3) in the energy landscape are shortcuts not taken by the actual dynamics. Hence the straightforward application of our method would yield suboptimal results for mobilities other than (1.3), even though we believe that the coarsening rate for $M(h) = h^3$ is the same as for $M(h) = h$.

In view of (1.2) and (1.3), equation (1.1) turns into

$$\partial_t h + \nabla \cdot \big(h \nabla \big(\Delta h - \mathcal{U}'(h)\big)\big) \;=\; 0 \quad \text{ in } (0,\infty) \times Q. \tag{1.4a}$$

As suitable boundary conditions, we take equilibrium and no-flux boundary conditions:

$$\nu \cdot \nabla h = \nu \cdot \nabla \left(\frac{\partial E}{\partial h} \right) \;=\; 0 \quad \text{ on } (0,\infty) \times \partial Q. \tag{1.4b}$$

These boundary conditions ensure that the total mass $\int h \, dx$ is conserved and that the total energy $E(h)$ decreases over time:

$$\frac{d}{dt} \int h \, dx \;=\; 0,$$

$$\frac{d}{dt} E \;=\; - \int h \Big| \nabla \left(\frac{\partial E}{\partial h} \right) \Big|^2 \, dx \;\leq\; 0.$$

A glance at the energy functional E, and $\mathcal{U}$ in particular, reveals that there is a characteristic scale for x and h, both normalized to order one. We are interested in very large systems, i.e.

$$Q = (0, \Lambda)^n \text{ with } \Lambda \gg 1.$$

We focus on initial data which are within the unstable range:

$$h \;\approx\; \text{const} \quad \text{ with } \quad \mathcal{U}''(h) < 0$$

and whose height is of the order of the precursor layer, i.e.

$$h \;\sim\; 1.$$

Our numerical simulations reveal the generic behavior of the evolution. After an initial stage, a configuration of well-defined droplets connected by a precursor layer of height $h \approx 1 = \operatorname{argmin} \mathcal{U}$ emerges. From then onwards, the large droplets grow at the expense of the small ones via mass exchange through the precursor layer. Eventually, the smaller droplets disappear. Figure 2 shows a typical evolution of the film height. In a sufficiently large systems, this coarsening process seems statistically self-similar. It is driven by the reduction of total energy E. Our main result gives a lower bound on the rate by which the energy decreases.

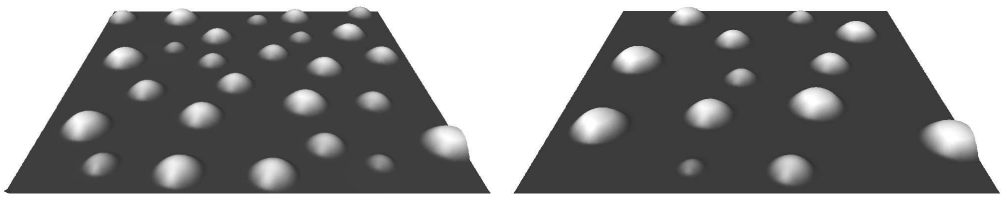

Figure 2: Plots of numerically computed height of the liquid on a two-dimensional substrate at two different times.

We shall see that E not only is a Lyapunov functional for (1.4), but that (1.4) can in fact be interpreted as a gradient flow of (1.2), see Appendix B. For

our analysis, we need a measure of the distance in the configuration space, i.e. a way to express how far two droplet configurations h_0, h_1 are. It is natural to take the distance which is given by the gradient flow structure. As motivated in Appendix B, that distance is the Wasserstein distance $\mathcal{W}(h_0, h_1)$:

$$\mathcal{W}(h_0,h_1)^2 \;:=\; \inf\left\{\iint |x-y|^2 d\pi(x,y) \;\Big|\; \int d\pi(\cdot,y) = h_0,\ \int d\pi(x,\cdot) = h_1\right\}. \tag{1.5}$$

The so-called transportation plan, π, is a measure on the product space $Q \times Q$. It is admissible if its projections to first and second coordinates are measures with densities h_0 and h_1, respectively. The transportation cost is measured by the squared Euclidean distance $|x-y|^2$. For properties of $\mathcal{W}$ see Section 7.1 in [32].

We are now in the position to formulate our result:

Theorem 1. *Let $\mathcal{U}$ satisfy*

$$\begin{array}{ll} \mathcal{U}(h) \geq 0 & \text{on } (0,\infty), \\ \mathcal{U}(h) \geq 1 & \text{on } (2,\infty). \end{array} \tag{1.6}$$

Let h be a smooth solution of (1.4), which has the same total volume as a constant layer of thickness 3:

$$\int h\, dx \;=\; \int h^*\, dx, \quad h^* \equiv 3. \tag{1.7}$$

Then for $\sigma \in (1, \frac{3n+2}{n})$

$$\int_0^T \left(\Lambda^{-n} E(h(t))\right)^\sigma \, dt \quad \gtrsim \quad \int_0^T (t^{-\frac{n}{3n+2}})^\sigma \, dt, \tag{1.8}$$

provided $T \gg \left(\Lambda^{-\frac{n}{2}} \mathcal{W}(h^*, h(0))\right)^{\frac{3n+2}{n+1}}$ and $\Lambda^{-n} E(h(0)) \ll 1$.

For the precise meaning of the notation "$\gg$" and "$\gtrsim$" we refer to Remark 1 in Section 2. The result states that the energy per volume cannot decrease faster than $t^{-\frac{n}{3n+2}}$. For further interpretation of the result in terms of the droplet configuration we refer to Subsection 1.4. The assumption $\Lambda^{-n} E(h(0)) \ll 1$ of small energy densities encodes that $h(0)$ energetically behaves as a configuration of droplets connected by a precursor layer of height argmin $\mathcal{U} = 1$, see Figure 2. This means that we "start the clock" once the system has entered such a regime. The assumption $T \gg \left(\Lambda^{-\frac{n}{2}} \mathcal{W}(h^*, h(0))\right)^{\frac{3n+2}{n+1}}$, on the other hand, ensures that the initial data $h(0)$ are not too far from a constant film thickness. The values 1, 2 and 3 in (1.6) and (1.7) are set purely for convenience. In particular, given a potential satisfying (1.6), any constant layer of thickness above 2 is admissible. However, the constants in the estimates would depend on the thickness.

The framework for proving lower bounds on energy decay was introduced by Kohn and one of the authors in [10] for the constant-mobility and the degenerate-mobility Cahn-Hilliard equation. The basic idea is to use the gradient flow structure of (1.4). A gradient flow structure is determined by the energy functional E and a (Riemannian) geometry of the state space (the space

of all droplet configurations h). The metric tensor encodes the relevant dissipation mechanism, see Appendix B. Following [10], we use coarse information on the geometry of the energy landscape to derive coarse information on the gradient flow dynamics. The coarse information on geometry is how fast E can decrease as a function of the distance to a reference configuration h^*, where the function is given by a power law with the "geometric exponent" α, see Figure 3. On the other hand, the coarse information on dynamics limits how fast E can decrease as a function of time, where the function is given by a power law with the "dynamic exponent" γ. Proposition 1 in Section 2 relates the dynamic exponent γ to the geometric exponent α.

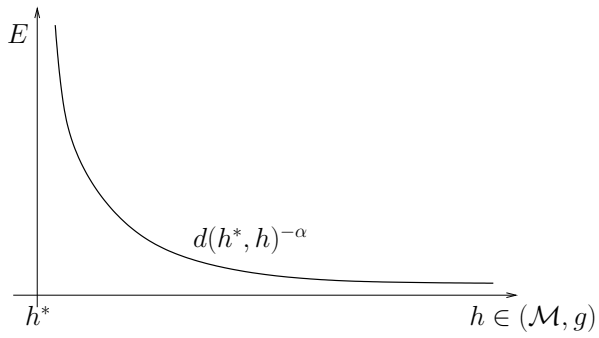

Figure 3: The energy $E(h)$ is bounded below by the distance between h and the reference state h^*.

Let us point out that studying *lower* bounds on the coarsening rate is a more complicated question. In fact, there are solutions which do not coarsen at all; for example the unstable, periodic steady states. Hence a lower bound can only hold in some generic sense — a statement for all trajectories cannot hold. We do not address this issue.

Other applications of the method proposed in [10] can be found in the literature. In [3], coarsening in off-critical mixtures within the Mullins-Sekerka evolution is studied. The authors of [4] and [5] study the coarsening behavior in mean-field models of phase transitions and of a phase-field model that deals with both temperature and phase fields. In [11] and [12], rigorous bounds on coarsening rates are proven for an epitaxial growth model and for models of multicomponent phase separation.

1.2. **Outline.** The following subsections provide background information: In Subsection 1.3, we describe the underlying physical processes. Heuristics, which further interpret the result in Theorem 1, are presented in Subsection 1.4. Formal asymptotics, e.g. done for the one-dimensional case in [6], are shortly reviewed in Subsection 1.5. In Subsection 1.6, we present our numerical experiments which support that the power law bounds we obtain are optimal for $n = 1$ and $n = 2$. The proof of Theorem 1 does not depend on the results presented in these subsections.

In Section 2, we review the abstract framework, which exploits the gradient flow structure to obtain a bound on the energy, proposed in [10], and give modified proofs of the main results. Our main contribution is the interpolation inequality, which is essential for the framework. From the mathematical point of view, it is an extension of the one established in [3]. We rigorously state and prove the inequality in Section 3. Section 4 provides the proof of the main result. Appendix A contains the analysis of stationary droplets, while Appendix B explains the gradient flow structure of the thin-film equation. The Wasserstein metric, as the induced distance, is introduced heuristically.

1.3. **Physics.** The statics is determined by capillarity (the surface tension between liquid and vapor) and the short range forces between the film and the solid substrate. These intermolecular forces are the combination of a very short-range repulsive (Born-type) force and a moderately short-range attractive (van der Waals) force. Their competition stabilizes a precursor layer of well-defined height, which covers the entire substrate. In particular, our choice of $\mathcal{U}$ with $\operatorname{argmin}\mathcal{U} = 1$ yields a precursor layer of height ≈ 1. On a more mesoscopic level, the liquid is partially wetting: It allows for equilibrium droplets of a well-defined apparent (i. e. mesoscopic) contact angle. The apparent non-zero contact angle arises from the competition between the short range forces and capillarity.

Intermolecular forces of the form discussed above are relevant for a range of liquids: polymers [1, 26, 27, 28, 29, 33], liquid crystal films and liquid metals [8, 31], evaporating films [19], and others.

The dynamics is driven by the reduction of total energy (capillary and intermolecular). The reduction of energy is limited by viscous friction. This dissipation mechanism is rather pronounced in the thin liquid film. This means that inertial effects are negligible and the dynamics are determined by a quasi-stationary balance of thermodynamic driving and viscous frictional forces. Notice that the presence of the precursor layer removes the singularity of the moving contact line which arises from the no-slip boundary condition.

We think of the initial condition as a flat film of a height sufficiently large with respect to the equilibrium height of the precursor layer. More precisely, we think of a perturbation of this configuration; due to the intermolecular forces, sufficiently long-wave length perturbations grow. In analogy with spinodal decomposition of binary mixtures (as described by the Cahn–Hilliard equation) this process is often referred to as spinodal dewetting. The liquid film almost ruptures and holes (with film thickness of the precursor layer) surrounded by a network of ridges form. This initial process may have various morphologies [1, 30]. As time passes, the ridges break up and relax to droplets sitting on the precursor layer. In this paper, we are not concerned with this initial stage of droplet formation.

We are interested in the late-stage *coarsening* behavior. A configuration of well-separated droplets connected by a precursor layer coarsens in time, see Figure 2. We have in mind a scenario with clearly separated time scales: The

time scale of the coarsening process is slow compared to the scale on which the droplets relax to equilibrium shape. Hence the configuration is essentially described by the radius and the position of the center of mass of the individual droplets. These quantities evolve slowly. This is sometimes called quasi-static evolution or quasi-stationary motion.

The coarsening process can be mediated by two mechanisms: collapse or collision. Collapse relies on mass exchange between the droplets through the precursor layer. In this scenario, the large droplets grow at the expense of the small ones which eventually collapse. This is a particular instance of Ostwald ripening. The basic difference with respect to the traditional Ostwald ripening for binary mixtures (as described by the late stages of the Cahn–Hilliard equation with strongly off-critical initial data, see for instance [18] for the two-dimensional case) lies in the mixed dimensionality: Ripening of droplets on an n-dimensional substrate is $(n+1)$-dimensional with respect to mass and energy, but n-dimensional when it comes to the kinetics.

We now address collision: As do the particles in traditional Ostwald ripening, the droplets drift. The difference with respect to traditional Ostwald ripening lies in the fact that droplets are much more mobile than particles (since the mobility strongly depends on height). In [6], it has been argued that on a one-dimensional substrate, this effect may lead to collision and thus to "accidental" coarsening.

Unlike for the initial instability and subsequent dewetting, there are few experimental studies of coarsening in liquid films. The only long-time results we are aware of are studies of coarsening for certain polymers [14, 15].

1.4. **Dynamical scaling: Heuristics.** Numerical simulations suggest that coarsening, although rather complex in detail, has a simple statistical behavior (see Section 1.6). In particular, the time-dependence of averaged quantities, like the average distance L between droplets, in sufficiently large systems appears to be a power law:

$$L \sim t^{\beta}.$$

We are interested in understanding the mechanisms which determine the characteristic exponent β. In order to discern what information about β is contained in the energy bound (1.8), we first analyze and relate the length scales present in the problem. We consider configurations of well-separated, equilibrium-shaped droplets with fixed average height greater than the height of the precursor layer. The typical averaged length scales are the typical distance L, the height H and radius R of a droplet. Figure 4 sketches such a typical droplet configuration we have in mind.

From this point of view, we infer the following scaling relations:

- On a mesoscopic level, the potential $\mathcal{U}$ acts as the characteristic function of $\{h > 1\}$. Thus the individual droplets are governed by the mesoscopic energy

$$\overline{E}(h) = \int \tfrac{1}{2}|\nabla h|^2 \, dx + \text{ vol}\,(\{h > 1\}),$$

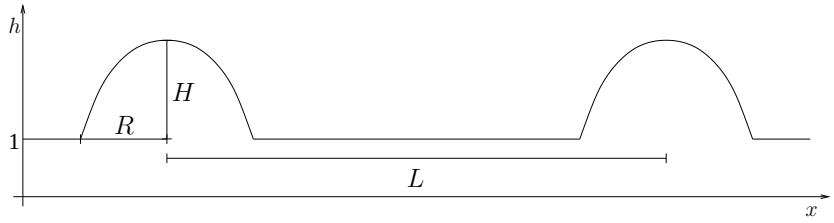

Figure 4: Droplet configuration on one-dimensional substrate. The typical length scales H, R and L are not independent, cf. (1.10) & (1.11).

which enforces an apparent equilibrium contact angle of

$$\tfrac{1}{2}|\nabla h|^2 = 1 \quad \text{on } \partial\{h > 1\}, \tag{1.9}$$

see Appendix A. Notice that (1.9) implies that the average height H and the average radius R of the droplets scale the same:

$$H \sim R. \tag{1.10}$$

- We infer from mass conservation, i.e.

$$\Lambda^{-n} \int h \, dx \sim 1,$$

and

$$\begin{aligned} \Lambda^{-n} \int h \, dx &\sim \left(\begin{array}{c} \text{number density} \\ \text{of droplets} \end{array} \right) \times \left(\begin{array}{c} \text{volume of} \\ \text{individual droplet} \end{array} \right) \\ &\sim L^{-n} \times H R^n \\ &\overset{(1.10)}{\sim} L^{-n} \times R^{n+1} \end{aligned}$$

that R and L are related by

$$L \sim R^{\frac{n+1}{n}}. \tag{1.11}$$

Now let us explain why a lower bound on the energy heuristically yields an upper bound on the average droplet distance L. Indeed, the energy density (i.e. the energy per system volume) is related to L via

$$\begin{aligned} \Lambda^{-n} E &\sim \left(\begin{array}{c} \text{number density} \\ \text{of droplets} \end{array} \right) \times \left(\begin{array}{c} \text{energy of} \\ \text{individual droplet} \end{array} \right) \\ &\overset{(1.10)}{\sim} L^{-n} \times R^n \\ &\overset{(1.11)}{\sim} L^{-\frac{n}{n+1}}. \end{aligned} \tag{1.12}$$

Thus a lower bound on E heuristically yields an upper bound on L. The energy bound (that we show in a time-averaged form in Theorem 1)

$$\Lambda^{-n} E \gtrsim t^{-\frac{n}{3n+2}}$$

in view of (1.12), heuristically amounts to the upper bound

$$\beta \;\leq\; \frac{n+1}{3n+2} \;=\; \begin{cases} \frac{2}{5} & \text{for } n=1 \\ \frac{3}{8} & \text{for } n=2 \end{cases}. \tag{1.13}$$

Based on numerical and heuristic predictions (which are solid for $n = 1$ and somewhat less so for $n = 2$) this bound is optimal (up to logarithmic correction in two dimensions). In the non-physical case of $n \geq 3$, we do not expect the bound to be optimal.

1.5. **Formal asymptotics.** The coarsening process on one-dimensional substrates was analytically studied by Glasner and Witelski [6, 7] for physically relevant mobility h^3. Based on the quasi-static assumption, they derive a system of coupled ODE-s for droplet pressures $\{P_i\}$ (which are in one-to-one correspondence to their radius) and droplet positions $\{X_i\}$. Using the scale separation $H \sim R \ll L$ they argue heuristically that

$$L \;\sim\; t^{\frac{2}{5}}.$$

Their numerical experiments confirm this scaling. Furthermore, Glasner and Witelski show that in certain regimes, both collapse and collisions of droplets are possible mechanisms of coarsening.

We verified that their heuristics extends to our mobility $M(h) = h$ and yields the same scaling. It is a particularity of the mobility $M(h) = h^3$ that both processes, collapse and collision, yield the same exponent (modulo a logarithm). For $M(h) = h$ however, collapse is eventually the faster process.

A back-of-the-envelope argument for two-dimensional substrates based on the collapse scenario suggests that

$$L \;\sim\; t^{\frac{3}{8}}$$

(modulo a logarithm specific to the fundamental solution of Laplace equation in 2-d, see [18]). The importance of collisions, as it depends on $M(h)$, is not yet well-understood in our opinion, despite the investigation of droplet mobility in [25].

Our analysis does not rely on a derivation of a reduced model based on a quasi-static assumption. Likewise, it does not presuppose that coarsening is simple on a statistical level.

1.6. **Numerics.** To gain some understanding of the coarsening dynamics we carried out several numerical experiments. Let us first address the discretization of the thin-film equation (1.4). To solve this equation (1.4) in one and two dimensions we use a modification of the discretization of a Cahn–Hilliard-type equation proposed in [21]. This discretization approach is guided by two features of the model (1.4):

- The total mass $\int h$ is preserved due to the continuity equation

$$\partial_t h + \nabla \cdot J \;=\; 0, \tag{1.14}$$

  where $J = -h\nabla\left(\frac{\partial E}{\partial h}\right)$.

- The energy E is a Lyapunov functional:

$$\frac{d}{dt}E \;=\; -\int \frac{1}{h}|J|^2 \;\leq\; 0.$$

We use a semi-implicit time discretization (explicit in the mobility). Since the time-discrete equation is non-linear we apply a single Newton step:

$$h^{k+1}-h^k-\tau\nabla\cdot\left[h^k\nabla\left(\frac{\partial^2 E}{\partial h^2}(h^k)(h^{k+1}-h^k)+\frac{\partial E}{\partial h}(h^k)\right)\right] \;=\; 0.$$

By introducing the flux J:

$$h^{k+1} \;=\; h^k-\tau\nabla\cdot J^{k+1},$$

we obtain a symmetric problem

$$\left[\frac{1}{h^k}\mathrm{id}-\tau\nabla\left(\frac{\partial^2 E}{\partial h^2}(h^k)\right)\nabla\cdot\right]J^{k+1}=-\frac{1}{h^k}\nabla\left(\frac{\partial E}{\partial h}(h^k)\right).$$

We use a finite difference scheme for the fourth-order problem and solve the linear system by conjugate gradient method, preconditioned by the constant coefficient operator $\mathrm{id}-\tau\nabla\left(\frac{\partial^2 E}{\partial h^2}(1)\right)\nabla\cdot$, which we invert by FFT.

Now we turn to the numerical experiments. We use the potential

$$\mathcal{U}(h)=2h^{-3}-3h^{-2}+1,$$

which was used in [6, 19], and take as initial data

$$h(t=0)=h^*+\text{perturbation},$$

where we choose $h^*\equiv 2$, which is in the concave part of $\mathcal{U}$, but still of the order of the precursor layer thickness. System sizes are chosen $\Lambda=10000$ for $n=1$ and $\Lambda=1000$ for $n=2$.

Figure 6 shows a logarithmic plot of the number of droplets vs. time both in one and two dimension. Furthermore, we measure the energy density of the configurations, see Figure 5. Note that the data is averaged over ten runs.

Our numerical experiments reveal the scaling exponent $\beta=\frac{2}{5}$ for $n=1$ (see Figure 6 left), since the number density $\Lambda^{-n}N$ scales like L^{-n}. This exponent is equal to the upper bound we obtained in (1.13). Experiments for $n=2$ (see Figure 6 right) suggest a faster decrease of the number density than for $n=1$, as predicted. The coarsening exponent is in agreement with the bound (1.13), but appears to be slightly different than the bound itself. Let us comment on this apparent discrepancy: The heuristics in Subsection 1.4 are based on the assumption that

$$\begin{aligned}\Lambda^{-n}E &\overset{(1.12)}{\sim} L^{-\frac{n}{n+1}}\\ &\sim \left(\Lambda^{-n}N\right)^{\frac{1}{n+1}}.\end{aligned}$$

We therefore monitor the system averaged quantity

$$\Lambda^{-n}E\left(\Lambda^{-n}N\right)^{-\frac{1}{n+1}}$$

over time. For an infinite system this number should reach an asymptotic value if coarsening is statistically self-similar. Figure 7 shows that for $n = 2$ the numerical simulations have barely reached an asymptotic state. Hence for $n = 2$ a numerical confirmation of the optimality of our result would require much larger time horizons and thus much larger system sizes.

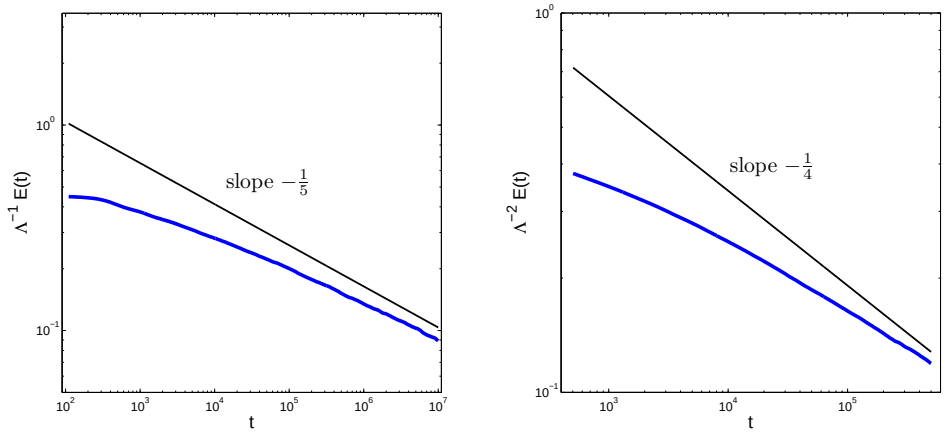

Figure 5: Energy density of droplet configuration for $n = 1$ (left) and for $n = 2$ (right) vs. time.

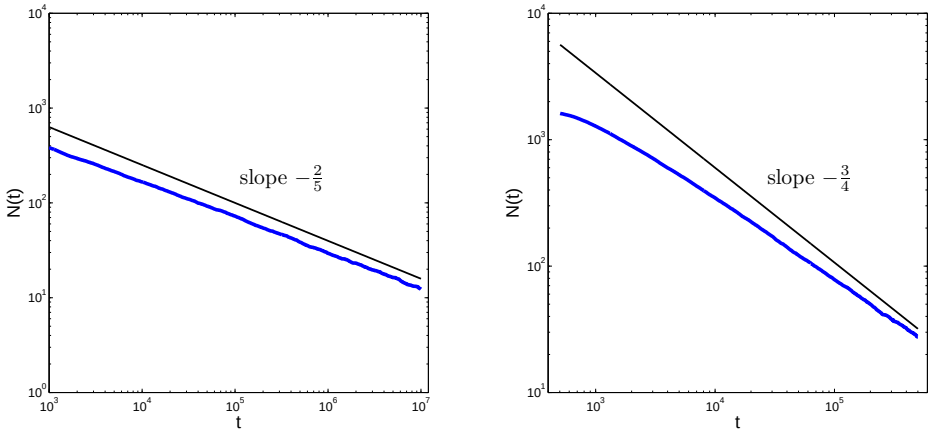

Figure 6: Number of droplets for $n = 1$ (left) and for $n = 2$ (right) vs. time.

2. Abstract framework: From geometry to dynamics

In this section we show how coarse information on the *geometry* of the energy landscape (see Figure 3) leads to coarse information on the gradient flow *dynamics*. Proposition 1 relates the dynamic exponent γ to the geometric exponent

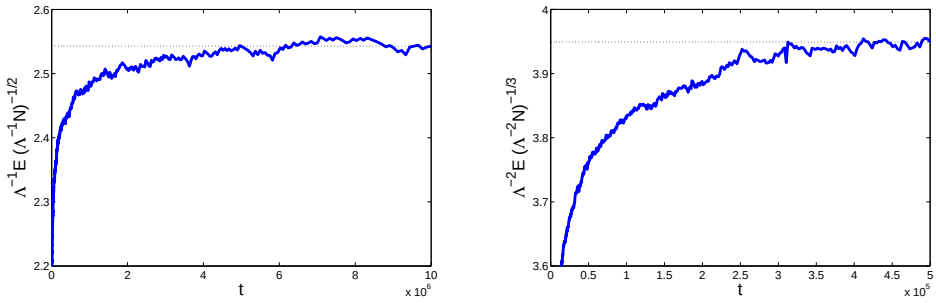

Figure 7: The system averaged quantity $\Lambda^{-n}E\,(\Lambda^{-n}N)^{-\frac{1}{n+1}}$ for $n=1$ (left) and for $n=2$ (right) vs. time.

α:

$$\gamma \;=\; \frac{\alpha}{\alpha+2}.$$

This insight is essentially from [10]. We give a somewhat different presentation here and include the modified proofs for the convenience of the reader. For the clarity of presentation, we adopt an abstract framework: Let $\mathcal{M}$ be a manifold endowed with a metric tensor g and a function E. We denote by d the induced distance on the Riemannian manifold $(\mathcal{M},g)$.

Proposition 1 ([10]). *Let $h^*\in\mathcal{M}$. Let $h:\mathbb{R}_+\to\mathcal{M}$ be a solution of*

$$\partial_t h \;=\; -\mathrm{grad}E(h). \tag{2.1}$$

and $h(0)=h_0$.

Assume that for some $\alpha>0$ the interpolation inequality

$$E(h)d(h,h^*)^\alpha \geq 1 \quad \text{for all } h\in\mathcal{M} \text{ with } E(h)\leq 1 \tag{2.2}$$

holds. Then for $\sigma\in(1,1+\frac{2}{\alpha})$

$$\int_0^T E(h(t))^\sigma\,dt \gtrsim \int_0^T (t^{-\frac{\alpha}{\alpha+2}})^\sigma\,dt \tag{2.3}$$

provided $T\gg d(h_0,h^*)^{\alpha+2}$ and $E(h(0))\leq 1$.

Remark 1. *The notation $\gtrsim$ and $\gg$ stands for:*

For all $\sigma\in(1,1+\frac{2}{\alpha})$ there exists a constant $C=C(\alpha,\sigma)$ such that $\forall\delta>0$ $\exists C_\delta=C(\alpha,\sigma,\delta)$:

$$\int_0^T E(h(t))^\sigma\,dt \geq (1-\delta)C\int_0^T (t^{-\frac{\alpha}{\alpha+2}})^\sigma\,dt \tag{2.4}$$

provided $T\geq C_\delta d(h_0,h^*)^{\alpha+2}$.

Remark 2. *It is not true that (2.1) and (2.2) imply the pointwise estimate*

$$E(t) \;\gtrsim\; t^{-\frac{\alpha}{\alpha+2}}. \tag{2.5}$$

Indeed, let $\mathcal{M} = \mathbb{R}_+$, $h^* = 0$ and $h(0) = 1$. For given $b \gg 1$ let E_b be equal to $h^{-\alpha}$ outside the interval $(1, b)$ and let it be linear on $[1, b]$ so that E_b is continuous:

$$E_b(h) := \begin{cases} 1 + \frac{b^{-\alpha}-1}{b-1}(h-1) & \text{on } [1,b], \\ h^{-\alpha} & \text{otherwise.} \end{cases}$$

Then

$$\partial_t h \;=\; -\frac{dE_b}{dh}(h(t)) = -\frac{b^{-\alpha}-1}{b-1}$$

as long as $h(t) \le b$. Hence

$$h(t) = 1 - \frac{b^{-\alpha}-1}{b-1}t$$

and thus $h(t_b) = b$ for $t_b := \frac{(b-1)^2}{1-b^{-\alpha}}$. Therefore

$$\frac{E_b(h(t_b))}{t_b^{-\frac{\alpha}{\alpha+2}}} \;=\; \frac{(b-1)^{\frac{2\alpha}{\alpha+2}}}{b^\alpha (1-b^{-\alpha})^{\frac{\alpha}{\alpha+2}}} \;\le\; 2b^{-\frac{\alpha^2}{\alpha+2}} \to 0$$

as $b \to \infty$.

Remark 3. *The range for $1 < \sigma < 1 + \frac{2}{\alpha}$ is (almost) optimal.*

The example above can be used to show that for $0 < \sigma < 1$ the statement cannot hold. An elementary (but lengthy) calculation shows that for $T = b^{2+\alpha-\eta}$, with $0 < \eta < \alpha(1-\sigma)$

$$\int_0^T (E_b(h(t)))^\sigma dt \sim b^{2+\alpha(1-\sigma)-\eta},$$
$$\int_0^T t^{-\frac{\alpha\sigma}{\alpha+2}} dt \sim b^{2+\alpha(1-\sigma)-\eta+\frac{\alpha\sigma\eta}{\alpha+2}}.$$

Thus inequality (2.3) cannot hold when $0 < \sigma < 1$. The case $\sigma = 1$ remains open. The proof we present for $\sigma > 1$ does not extend to $\sigma = 1$ since the constant C in (2.4) vanishes as σ approaches 1; see (2.12).

For $\sigma = 1 + \frac{2}{\alpha}$ the statement would hold if the lower bound 0 in the integrals was replaced by 1. This follows from the continuity of the functionals with respect to σ and from the fact that constant C is bounded away from 0 as σ approaches $1 + \frac{2}{\alpha}$; see (2.12). The range $\sigma > 1 + \frac{2}{\alpha}$ is not of interest, since the integral from 1 to infinity of the right hand side is finite, and hence the inequality (2.3) would contain no information on the decay rate of E.

We now consider an arbitrary but fixed trajectory $h(t)$ of (2.1). The following lemma restricts the rate at which the distance $d(h, h^*)$ between $h(t)$ and any fixed $h^* \in \mathcal{M}$ can change. We set for convenience

$$\begin{aligned} E(t) &:= E(h(t)) \\ D(t) &:= d(h(t), h^*). \end{aligned}$$

Lemma 1. *Let h be a solution of (2.1) and $h^* \in \mathcal{M}$.*
Then

$$\left|\tfrac{d}{dt}D(t)\right|^2 \;\le\; -\tfrac{d}{dt}E(t). \tag{2.6}$$

Proof of Lemma 1. The triangle inequality and the definition of d imply for any $\delta \in \mathbb{R}$

$$\begin{aligned}\left|\frac{1}{\delta}(D(t+\delta)-D(t))\right| &\le \frac{1}{\delta}d(h(t+\delta),h(t))\\ &\le \frac{1}{\delta}\int_0^1 \sqrt{g_{h(t+s\delta)}(\partial_t h(t+s\delta)\delta,\partial_t h(t+s\delta)\delta)}\,ds\\ &= \int_0^1 \sqrt{g_{h(t+s\delta)}(\partial_t h(t+s\delta),\partial_t h(t+s\delta))}\,ds.\end{aligned}$$

Hence we obtain in the limit $\delta \to 0$

$$\left|\frac{d}{dt}D(t)\right| \;\le\; \sqrt{g_{h(t)}(\partial_t h(t),\partial_t h(t))}.$$

Furthermore

$$\tfrac{d}{dt}E(t) = g_{h(t)}(\mathrm{grad}E(t),\partial_t h(t)) \overset{(2.1)}{=} -g_{h(t)}(\partial_t h(t),\partial_t h(t)),$$

so that we conclude

$$\left|\tfrac{d}{dt}D(t)\right|^2 \;\le\; -\tfrac{d}{dt}E(t).$$

□

Proof of Proposition 1. Since E is a monotone function of time, $D(t)$ can be viewed as a function of $E(t)$. To distinguish the argument of this function from the actual value of the energy we write $D = D(e)$. Hence (2.6) turns into

$$1 \;\ge\; \left(\frac{dD}{de}\right)^2 |\dot{E}|. \tag{2.7}$$

Multiplying (2.7) by $E(t)^\sigma$ and integrating in t yield

$$\int_0^T E(t)^\sigma\,dt \ge \int_0^T E(t)^\sigma \left(\frac{dD}{de}\right)^2 |\dot{E}|\,dt = \int_{E_T}^{E_0} e^\sigma \left(\frac{dD}{de}\right)^2 de, \tag{2.8}$$

where we have set $E_0 = E(0)$ and $E_T = E(T)$.

From the Cauchy–Schwarz inequality we obtain

$$\left(\int_{E_T}^{E_0} e^\sigma \left(\frac{dD}{de}\right)^2 de \int_{E_T}^{E_0} e^{-\sigma}\,de\right)^{\frac{1}{2}} \;\ge\; \left|\int_{E_T}^{E_0} \frac{dD}{de}\,de\right| \;=\; |D_0 - D_T|,$$

where we define $D_0 = D(0)$ and $D_T = D(T)$. Substituting in (2.8) and integrating $\int_{E_T}^{E_0} e^{-\sigma}\,de = (\sigma-1)^{-1}\left(E_T^{1-\sigma} - E_0^{1-\sigma}\right)$ implies

$$\begin{aligned}\int_0^T E(t)^\sigma\,dt &\ge (\sigma-1)\left(E_T^{1-\sigma}-E_0^{1-\sigma}\right)^{-1}(D_0-D_T)^2\\ &\ge (\sigma-1)E_T^{\sigma-1}(D_0-D_T)^2.\end{aligned} \tag{2.9}$$

Here we have used the assumption $\sigma > 1$. We rewrite the right hand side of (2.9) as

$$(\sigma-1)E_T^{\sigma-1-\frac{2}{\alpha}}(E_T D_T^\alpha)^{\frac{2}{\alpha}}(1-\tfrac{D_0}{D_T})^2$$

and apply the interpolation inequality (2.2), so that

$$\int_0^T E(t)^\sigma \, dt \geq (\sigma-1)E_T^{\sigma-1-\frac{2}{\alpha}}(1-\tfrac{D_0}{D_T})^2. \tag{2.10}$$

Set for abbreviation

$$f(T) := \int_0^T E(t)^\sigma \, dt.$$

Then (2.10) turns into

$$\begin{aligned} f(T) &\geq (\sigma-1)f'(T)^{(\sigma-1-\frac{2}{\alpha})/\sigma}(1-\tfrac{D_0}{D_T})^2 \\ &= (\sigma-1)f'(T)^{\frac{\sigma\alpha-\alpha-2}{\sigma\alpha}}(1-\tfrac{D_0}{D_T})^2, \end{aligned}$$

or equivalently,

$$f(T)^{\frac{\sigma\alpha}{\alpha+2-\sigma\alpha}} f'(T) \geq \left((\sigma-1)(1-\tfrac{D_0}{D_T})^2\right)^{\frac{\sigma\alpha}{\alpha+2-\sigma\alpha}},$$

provided $\sigma < 1+\frac{2}{\alpha}$. Note that

$$f(T)^{\frac{\sigma\alpha}{\alpha+2-\sigma\alpha}} f'(T) = \frac{d}{dt}\left(\frac{f(T)^{\frac{\sigma\alpha}{\alpha+2-\sigma\alpha}+1}}{\frac{\sigma\alpha}{\alpha+2-\sigma\alpha}+1}\right) = \frac{d}{dt}\left(\frac{f(T)^{\frac{\alpha+2}{\alpha+2-\sigma\alpha}}}{\frac{\alpha+2}{\alpha+2-\sigma\alpha}}\right).$$

Then we get by integration in time

$$f(T) \geq (\sigma-1)^{\frac{\sigma\alpha}{\alpha+2}}\left(\tfrac{\alpha+2}{\alpha+2-\sigma\alpha}\right)^{1-\sigma\frac{\alpha}{\alpha+2}} (1-\tfrac{D_0}{D_T})^{2\frac{\sigma\alpha}{\alpha+2}} \, T^{1-\sigma\frac{\alpha}{\alpha+2}}. \tag{2.11}$$

When T is such that $\frac{D_0}{D_T} \leq 1-(1-\delta)^{\frac{\alpha+2}{2\sigma\alpha}} =: \varepsilon(\delta)$, equation (2.11) yields

$$f(T) \geq C(\alpha,\sigma)(1-\delta)\, T^{1-\sigma\frac{\alpha}{\alpha+2}}$$

with

$$C(\alpha,\sigma) := (\sigma-1)^{\frac{\sigma\alpha}{\alpha+2}}\left(\tfrac{\alpha+2}{\alpha+2-\sigma\alpha}\right)^{1-\sigma\frac{\alpha}{\alpha+2}}. \tag{2.12}$$

For the case $\frac{D_0}{D_T} > \varepsilon(\delta)$ the interpolation inequality yields

$$E_T^\sigma > \varepsilon(\delta)^{\sigma\alpha} D_0^{-\sigma\alpha}.$$

Since the energy decreases in time this inequality holds for all $t \leq T$, so that

$$\int_0^T E(t)^\sigma \, dt \geq \varepsilon(\delta)^{\sigma\alpha} D_0^{-\sigma\alpha} T = \varepsilon(\delta)^{\sigma\alpha} D_0^{-\sigma\alpha} T^{\sigma\frac{\alpha}{\alpha+2}} \, T^{1-\sigma\frac{\alpha}{\alpha+2}}.$$

Hence

$$f(T) \;\geq\; (1-\delta)C(\alpha,\sigma)\, T^{1-\sigma\frac{\alpha}{\alpha+2}}$$

provided $T \geq C(\alpha,\sigma)^{\frac{\alpha+2}{\sigma\alpha}}\varepsilon(\delta)^{-\alpha-2}\, D_0^{\alpha+2}$, which proves (2.4). □

Remark 4. *The coefficient C is optimal for $\sigma = 1+\frac{1}{\alpha}$.*

To see that the coefficient is optimal for $\sigma = 1+\frac{1}{\alpha}$, consider in 1-$d$ the energy $E(h) := h^{-\alpha}$. Obviously this energy obeys the interpolation inequality (2.2) for $h^* = 0$. The gradient flow of E with $h_0 = 0$ is given by

$$h(t) = (\alpha(\alpha+2)t)^{\frac{1}{\alpha+2}}.$$

Hence

$$E(h(t)) = h(t)^{-\alpha} = (\alpha(\alpha+2)t)^{-\frac{\alpha}{\alpha+2}}$$

and furthermore

$$\int_0^T E(t)^\sigma \, dt = (\alpha(\alpha+2))^{-\sigma\frac{\alpha}{\alpha+2}} \frac{\alpha+2}{\alpha+2-\sigma\alpha} \, T^{1-\sigma\frac{\alpha}{\alpha+2}}.$$

The coefficient coincides with the coefficient in (2.11) provided $\sigma = 1+\frac{1}{\alpha}$.

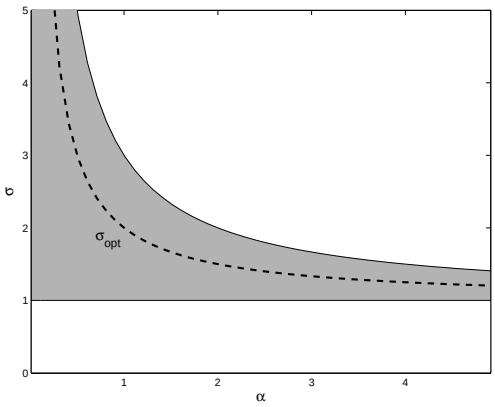

Figure 8: Permitted values of σ (grey region) as a function of α. The dotted line $\sigma_{\rm opt} := 1+\frac{1}{\alpha}$ indicates the values of σ for which the coefficient in (2.3) is optimal.

3. An interpolation inequality

From Section 2 and Appendix B we learn that relating the energy (1.2) and the induced distance (1.5) by an interpolation inequality of the form (1.12) provides a main ingredient for the proof of a lower bound on the energy. In view of Proposition 1, the geometric exponent α determines the dynamic exponent γ. As mentioned before, we fix $h^* \equiv 3$ to focus on ideas. Proposition 2 shows that the geometric exponent is $\alpha = \frac{n}{n+1}$.

Proposition 2. *There exists a constant $C > 0$ only depending on n such that*

$$\Lambda^{-n} E(h) \, \Big(\Lambda^{-\frac{n}{2}} \mathcal{W}(h,3)\Big)^{\frac{n}{n+1}} \geq \tfrac{1}{C} \qquad \textit{provided} \quad E(h) \leq \tfrac{1}{C}, \, \Lambda \geq C.$$

Before giving the rigorous proof, let us motivate the result. The exponent $\alpha = \frac{n}{n+1}$ can be heuristically inferred from the following argument:

- From (1.12) we have

$$\Lambda^{-n} E \ \sim \ L^{-\frac{n}{n+1}}.$$

- From the definition (1.5) of the Wasserstein distance $\mathcal{W}$ we obtain the scaling

$$\begin{aligned} \Lambda^{-n}\mathcal{W}(h,3)^2 &\sim \Lambda^{-n} \iint |x-y|^2 \, d\pi(x,y) \\ &\sim \Lambda^{-n} \times L^2 \iint d\pi(x,y) \\ &\sim \Lambda^{-n} \times L^2 \times \int 3 \, dx \\ &\sim L^2, \end{aligned}$$

(see Figure 9), that is,

$$\Lambda^{-\frac{n}{2}} \mathcal{W}(h,3) \ \sim \ L. \tag{3.1}$$

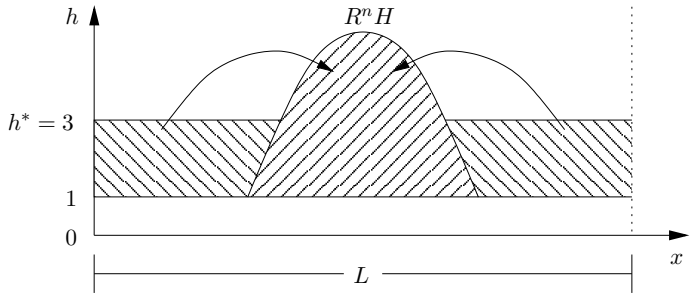

Figure 9: Scaling of $\mathcal{W}(h,3)$.

These two scaling relations yield

$$\Lambda^{-n} E \ \left(\Lambda^{-\frac{n}{2}} \mathcal{W}(h,3)\right)^{\frac{n}{n+1}} \ \sim \ L^{-\frac{n}{n+1}} \times L^{\frac{n}{n+1}} \ \sim \ 1.$$

We turn to the rigorous proof of Proposition 2. Set

$$R := (\Lambda^{-n} E(h))^{-1} \qquad \text{and} \qquad \widetilde{h} := (h-2)_+. \tag{3.2}$$

Note that the definition of R is motivated by the scaling (1.11) and (1.12). The proof is done in several lemmas:

- Lemma 2 shows that the average droplet height H scales like the average droplet radius in accordance with (1.10). The radius is expressed in terms of the energy, cf. (3.2).
- Lemma 3, applied to $\widetilde{h}$, shows that most of the droplet mass lies in a "small" set in the sense that the volume of the thickened set is controlled.

- Lemmas 2 and 3 imply Lemma 4, which shows that the typical droplet distance L scales like $R^{\frac{n+1}{n}}$, as suggested by the heuristic arguments in (1.11).
- Finally, Lemma 5 reveals that for sufficiently distant droplets the volume-averaged Wasserstein distance between h and the average height scales like L in accordance with (3.1).

Lemma 2.

(1) *The typical droplet height H is at least of order R in the sense that*

$$\int_{\{\widetilde{h}>H\}} \widetilde{h}\,dx \geq \tfrac{1}{2}\int \widetilde{h}\,dx \qquad \text{for } H=\tfrac{R}{2}. \tag{3.3}$$

(2) *The typical droplet radius is at least of the order R in the sense that*

$$R\int |\nabla \widetilde{h}|\,dx \leq \int \widetilde{h}\,dx. \tag{3.4}$$

Proof. We first notice that $h\leq \widetilde{h}+2$ implies

$$\int h\,dx \leq \int \widetilde{h}\,dx + \tfrac{2}{3}\int 3\,dx \overset{(1.7)}{=} \int \widetilde{h}\,dx + \tfrac{2}{3}\int h\,dx,$$

so that

$$\int \widetilde{h}\,dx \geq \tfrac{1}{3}\int h\,dx. \tag{3.5}$$

Next we notice that

$$\Lambda^{-n}E(h) \overset{(1.7)}{=} \tfrac{3}{\int h\,dx}\int \tfrac{1}{2}|\nabla h|^2+\mathcal{U}(h)\,dx \overset{(1.6)}{\geq} \tfrac{3}{\int h\,dx}\,\mathrm{vol}\,(\{h>2\}),$$

so that by (3.2)

$$\mathrm{vol}\,(\{h>2\}) \leq \tfrac{1}{3R}\int h\,dx. \tag{3.6}$$

This implies

$$\begin{aligned}\int_{\{\widetilde{h}\leq H\}} \widetilde{h}\,dx &= \int_{\{2<h\leq H+2\}} (h-2)\,dx\\ &\leq H\,\mathrm{vol}\,(\{h>2\})\\ &\overset{(3.6)}{\leq} \tfrac{H}{3R}\int h\,dx\\ &\overset{(3.5)}{\leq} \tfrac{H}{R}\int \widetilde{h}\,dx.\end{aligned}$$

Hence we obtain (3.3):

$$\int_{\{\widetilde{h}>H\}} \widetilde{h}\,dx = \int \widetilde{h}\,dx - \int_{\{\widetilde{h}\leq H\}} \widetilde{h}\,dx \geq \big(1-\tfrac{H}{R}\big)\int \widetilde{h}\,dx.$$

This motivates the choice of H.

Now we turn to (3.4):

$$\begin{aligned}\int |\nabla \widetilde{h}|\,dx &= \int_{\{h>2\}} |\nabla h|\,dx \\ &\overset{(1.6)}{\leq} \int |\nabla h|\sqrt{\mathcal{U}(h)}\,dx \\ &\leq \int \tfrac{1}{2}|\nabla h|^2 + \mathcal{U}(h)\,dx \\ &\overset{(1.7)}{=} \tfrac{\int h\,dx}{3\Lambda^n}\int \tfrac{1}{2}|\nabla h|^2 + \mathcal{U}(h)\,dx \\ &\overset{(3.5)}{\leq} \Lambda^{-n}E(h)\int \widetilde{h}\,dx.\end{aligned}$$

According to (3.2) this turns into

$$R\int |\nabla \widetilde{h}|\,dx \leq \int \widetilde{h}\,dx.$$

□

The next lemma is strongly inspired by [3, Lemma 2.1].

Lemma 3. *Let $R \leq \Lambda$. Assume $g : (0,\Lambda)^n \to [0,\infty)$*

- *has height H in the sense that*

$$\int_{\{g\geq H\}} g\,dx \geq \tfrac{1}{2}\int g\,dx \tag{3.7}$$

- *and radius R in the sense that*

$$R\int |\nabla g|\,dx \leq \int g\,dx. \tag{3.8}$$

Then there exists a set $A_R \subset \{g \geq H\}$

(1) *which contains substantial mass in the sense that*

$$\int_{A_R} g\,dx \geq \tfrac{1}{4}\int g\,dx$$

(2) *and is small in the sense that the volume of the thickened sets*

$$A_R^d := \{x \in (0,\Lambda)^n \mid \mathit{dist}(x, A_R) < d\}$$

is controlled by

$$\mathit{vol}\,(A_R^d) \leq 3^n 2^{n+1}\left(1+4\tfrac{d}{R}\right)^n \tfrac{1}{H}\int g\,dx \qquad \text{for all } d>0.$$

Proof. Extend $g : [0,\Lambda]^n \to \mathbb{R}$ to $\overline{g} : \mathbb{R}^n \to \mathbb{R}$ as follows:

- $[0,\Lambda]^n \rightsquigarrow [-\Lambda,\Lambda]^n$ by even reflection and
- $[-\Lambda,\Lambda]^n \rightsquigarrow \mathbb{R}^n$ by periodic continuation.

Set for convenience $\overline{A} := \{\overline{g} \geq H\}$. Define

$$\overline{A}_R := \left\{ x \in \overline{A} \;\middle|\; \int_{B(x,\frac{R}{8})} \overline{g}\,dy \geq \tfrac{H}{2}\,\mathrm{vol}\,(B(x,\frac{R}{8}))\right\}. \tag{3.9}$$

With the help of the convolution of $\overline{g}$

$$\overline{g}_R(x) := \frac{1}{\mathrm{vol}\,(B(x,\frac{R}{8}))}\int_{B(x,\frac{R}{8})} \overline{g}\,dy,$$

$\overline{A}_R$ can be written as $\overline{A}_R = \{x \in \overline{A} \mid \overline{g}_R(x) \geq \frac{H}{2}\}$.

We use the standard estimate

$$\int_{(-\Lambda,\Lambda)^n} |\overline{g} - \overline{g}_R|\,dx \leq \tfrac{R}{8}\int_{(-\Lambda,\Lambda)^n} |\nabla \overline{g}|\,dx \overset{(3.8)}{\leq} \tfrac{1}{8}\int_{(-\Lambda,\Lambda)^n} \overline{g}\,dx.$$

Since the integrands are even functions this yields

$$\int |g - \overline{g}_R|\,dx \leq \tfrac{1}{8}\int g\,dx. \tag{3.10}$$

We now define $A := \overline{A} \cap (0,\Lambda)^n$ and $A_R := \overline{A}_R \cap (0,\Lambda)^n$. Then we have

$$g \geq H \geq 2\overline{g}_R \quad \text{on } A - A_R$$

and thus

$$g \leq 2(g - \overline{g}_R) \quad \text{on } A - A_R.$$

Therefore

$$\int_{A-A_R} g\,dx \leq 2\int_{A-A_R} (g - \overline{g}_R)\,dx \leq 2\int |g - \overline{g}_R|\,dx \overset{(3.10)}{\leq} \tfrac{1}{4}\int g\,dx. \tag{3.11}$$

Notice that by assumption (3.7), $\int_A g\,dx \geq \frac{1}{2}\int g\,dx$. Hence

$$\begin{aligned}\int g\,dx &\leq 2\int_A g\,dx\\ &\leq 2\left(\int_{A_R} g\,dx + \int_{A-A_R} g\,dx\right)\\ &\overset{(3.11)}{\leq} 2\int_{A_R} g\,dx + \tfrac{1}{2}\int g\,dx,\end{aligned}$$

which yields the first assertion.

Let $J \subset A_R$ be maximal with the property

$$\left\{B(x,\tfrac{R}{8})\right\}_{x\in J} \text{ are disjoint.} \tag{3.12}$$

Then necessarily

$$A_R \subset \bigcup_{x\in J} B(x,\tfrac{R}{4}). \tag{3.13}$$

Thus

$$\begin{aligned} \#J \ \mathrm{vol}\,(B(0,\tfrac{R}{8})) &= \sum_{x\in J} \mathrm{vol}\,(B(x,\tfrac{R}{8})) \\ &\overset{(3.9)}{\leq} \tfrac{2}{H}\sum_{x\in J}\int_{B(x,\frac{R}{8})} \overline{g}\,dx \\ &\overset{(3.12)}{\leq} \tfrac{2}{H}\int_{(-\Lambda,2\Lambda)^n} \overline{g}\,dx \\ &= 3^n\tfrac{2}{H}\int g\,dx. \end{aligned} \tag{3.14}$$

Here we used the assumption $R \leq \Lambda$.

Now (3.13) implies $A_R^d \subset \bigcup_{x\in J} B(x, \frac{R}{4}+d)$, so that

$$\begin{aligned} \mathrm{vol}\,(A_R^d) &\leq \#J \ \mathrm{vol}\,(B(0,\tfrac{R}{4}+d)) \\ &= \frac{\mathrm{vol}\,(B(0,\frac{R}{4}+d))}{\mathrm{vol}\,(B(0,\frac{R}{8}))}\,\#J \ \mathrm{vol}\,(B(0,\tfrac{R}{8})) \\ &\overset{(3.14)}{\leq} 3^n(\tfrac{8}{R}(\tfrac{R}{4}+d))^n\tfrac{2}{H}\int g\,dx \\ &= 3^n 2^{n+1}(1+4\tfrac{d}{R})^n\tfrac{1}{H}\int g\,dx, \end{aligned}$$

which proves the second assertion. □

Lemma 4. *Let $\Lambda \geq R \geq 3^n 2^{8n}$. Then the typical droplet distance L is at least of the order $R^{\frac{n+1}{n}}$ in the following sense: There exists a set $A_R \subset \mathbb{R}^n$ such that*

(1)

$$\int_{A_R} h\,dx \geq \tfrac{1}{12}\int h\,dx, \tag{3.15}$$

(2)

$$3\ vol(A_R^L) \leq \tfrac{3}{4}\int_{A_R} h\,dx \quad \text{for } L = 3^{-1}2^{-10}R^{\frac{n+1}{n}}. \tag{3.16}$$

Proof. According to Lemma 3 there exists a set A_R such that

$$\int_{A_R} \widetilde{h}\,dx \geq \tfrac{1}{4}\int \widetilde{h}\,dx, \tag{3.17}$$

which by (3.5) turns into (3.15), and

$$\mathrm{vol}\,(A_R^L) \leq 3^n 2^{n+1}\left(1+4\tfrac{L}{R}\right)^n \tfrac{1}{H}\int \widetilde{h}\,dx. \tag{3.18}$$

By the definition of H and R in Lemma 2, (3.18) gives rise to

$$\begin{aligned}\mathrm{vol}\,(A_R^L) &\leq 3^n 2^{n+2}\left(1+4\tfrac{L}{R}\right)^n \tfrac{1}{R}\int \widetilde{h}\,dx\\ &\overset{(3.17)}{\leq} 3^n 2^{n+4}\left(1+4\tfrac{L}{R}\right)^n \tfrac{1}{R}\int_{A_R} \widetilde{h}\,dx\\ &\leq 3^n 2^{n+4}\left(1+4\tfrac{L}{R}\right)^n \tfrac{1}{R}\int_{A_R} h\,dx.\end{aligned}$$

Now L in (3.16) is defined such that

$$3^n 2^{n+4}\left(1+4\tfrac{L}{R}\right)^n \tfrac{1}{R} \leq \tfrac{1}{4}$$

provided $R \geq 3^n 2^{8n}$. Hence the inequality turns into

$$3\,\mathrm{vol}\,(A_R^L) \leq \tfrac{3}{4}\int_{A_R} h\,dx.$$

□

Lemma 5. *Let $h : Q \to [0,\infty)$ with $h^* := \Lambda^{-n}\int h(x)\,dx$ and $A \subset \mathbb{R}^n$ and $L > 0$ be given with*

$$h^*\ vol(\{dist(\cdot, A) < L\}) \leq \tfrac{3}{4}\int_A h(x)\,dx. \tag{3.19}$$

Then

$$\mathcal{W}(h,h^*)^2 \geq \tfrac{1}{4}L^2\int_A h(x)\,dx.$$

Proof. Set for abbreviation $A^L := \{\mathrm{dist}(.,A) < L\}$. Let π be any admissible transportation plan in the definition of $\mathcal{W}$. We conclude

$$\begin{aligned}\int_{\mathbb{R}^n\times\mathbb{R}^n} |x-y|^2\,d\pi(x,y) &\geq \int_{A\times(\mathbb{R}^n - A^L)} |x-y|^2\,d\pi(x,y)\\ &\geq L^2\pi(A\times(\mathbb{R}^n - A^L))\\ &\geq L^2(\pi(A\times\mathbb{R}^n) - \pi(\mathbb{R}^n\times A^L))\\ &= L^2\left(\int_A h\,dx - \int_{A^L} h^*\,dx\right)\\ &= L^2\left(\int_A h\,dx - h^*\,\mathrm{vol}\,(A^L)\right)\\ &\overset{(3.19)}{\geq} \tfrac{1}{4}L^2\int_A h\,dx.\end{aligned}$$

□

Proof of Proposition 2. According to Lemma 5 (applied to $h^* = 3$ and $A = A_R$) it follows from Lemma 4 for the L defined in (3.16)

$$\mathcal{W}(h,3)^2 \geq \tfrac{1}{4}L^2\int_{A_R} h\,dx \overset{(3.15)}{\geq} \tfrac{1}{48}L^2\int h\,dx.$$

In view of (1.7), this turns into

$$\Lambda^{-n}\mathcal{W}(h,3)^2 \geq 2^{-4}L^2.$$

In view of the definition (3.2) of R and the definition (3.16) of L this yields

$$\begin{aligned}\Lambda^{-n}E(h)\ \left(\Lambda^{-\frac{n}{2}}\mathcal{W}(h,3)\right)^{\frac{n}{n+1}} &\geq R^{-1}(2^{-4}L^2)^{\frac{n}{2(n+1)}}\\ &= R^{-1}(3^{-2}2^{-24}R^{2\frac{n+1}{n}})^{\frac{n}{2(n+1)}}\\ &= 3^{-\frac{n}{n+1}}2^{-\frac{12n}{n+1}}.\end{aligned}$$

□

4. Proof of Theorem 1

We cannot apply Proposition 1 right away since the argument for the (infinite-dimensional) gradient flow structure introduced in Appendix B is formal. An inspection of the proof of Proposition 1 reveals that it is only necessary to find a substitute for Lemma 1. In fact, one can directly prove the equivalent of Lemma 1 for the Wasserstein metric as defined in (1.5) and a smooth solution of (1.4).

Lemma 6. *Let h be a smooth solution of* (1.4)*. Then*

$$\left|\frac{d}{dt}\mathcal{W}(3,h(t))\right|^2 \ \leq\ \left(-\frac{d}{dt}E(t)\right). \tag{4.1}$$

Proof. We follow [22].

Note that

$$\frac{d}{dt}E(t) = -\int h\left|\nabla\frac{\partial E}{\partial h}\right|^2\ dx.$$

It thus is sufficient to establish the inequality

$$\left|\frac{d}{dt}\mathcal{W}(3,h(t))\right|^2 \ \leq\ \int h|u|^2\ dx \tag{4.2}$$

for the transport equation

$$\partial_t h + \nabla\cdot(hu)\ =\ 0. \tag{4.3}$$

Due to the triangle inequality we only need to show

$$\lim_{\delta\to 0}\frac{1}{\delta}\mathcal{W}(h_t,h_{t+\delta})\ \leq\ \sqrt{\int h_t|u_t|^2\ dx}. \tag{4.4}$$

Here, that the indices t and $t+\delta$ denote the time argument of h and u.

First we show that $h_{t+\delta}$ is the push-forward of h_t under the flow map Φ_δ generated by $u_{t+\delta}$, i.e.

$$\partial_\delta\Phi_\delta = u_{t+\delta}\circ\Phi_\delta, \qquad \Phi_0 = \mathrm{id}. \tag{4.5}$$

Note that by the push-forward one understands

$$\int\zeta\ h_{t+\delta}\ dx\ =\ \int(\zeta\circ\Phi_\delta)\ h_t\ dx \qquad \text{for all } \zeta\in C_0^0(\mathbb{R}^n). \tag{4.6}$$

For given ζ define $\zeta_\delta := \zeta \circ \Phi_\delta^{-1}$; ζ_δ satisfies

$$\partial_\delta \zeta_\delta + u_{t+\delta} \cdot \nabla \zeta_\delta \;=\; 0.$$

Furthermore, recall that $h_{t+\delta}$ solves the transport equation

$$\partial_\delta h_{t+\delta} + \nabla \cdot (h_{t+\delta} u_{t+\delta}) \;=\; 0.$$

Hence we obtain

$$\frac{d}{d\delta} \int \zeta_\delta \, h_{t+\delta} \, d\delta \;=\; \int (\partial_\delta \zeta_\delta \, h_{t+\delta} + \partial_\delta h_{t+\delta} \, \zeta_\delta) \, dx \;=\; 0,$$

which proves (4.6).

Next we define a product measure π_δ by

$$d\pi_\delta(x,y) \;=\; dh_t(x) \, \delta[y = \Phi_\delta(x)].$$

According to (4.6), π_δ defines an admissible transportation plan in the sense of the definition of $\mathcal{W}$. Thus we get by definition

$$\frac{1}{\delta} \mathcal{W}(h_t, h_{t+\delta}) \le \sqrt{\int \frac{1}{\delta^2} |x - \Phi_\delta(x)|^2 h_t(x) \, dx}.$$

We obtain from the definition (4.5) of the flow map that $\frac{1}{\delta^2}|x-\Phi_\delta(x)|^2$ converges pointwise to $|u_t|^2$. The dominated convergence theorem yields

$$\lim_{\delta \to 0} \int \frac{1}{\delta^2} |x - \Phi_\delta(x)|^2 h_t(x) \, dx \;=\; \int h_t |u_t|^2 \, dx,$$

which establishes (4.4). □

Appendix A. Stationary droplet shape

In this section, we analyze the shape of a stationary droplet. For this purpose we consider a single droplet with prescribed mass $V > 0$ on top of the precursor layer of equilibrium thickness $h \equiv 1$ on an n-dimensional substrate. We are interested in the stationary droplet shape on a mesoscopic scale. Hence we focus on the mesoscopic energy

$$\overline{E} = \int \tfrac{1}{2} |\nabla h|^2 \, dx + \; \mathrm{vol}\,(\{h > 1\}) \tag{A.1}$$

(see Section 1.4) for all h which fulfill the mass constraint

$$\int (h-1)_+ \, dx = V. \tag{A.2}$$

Since the precursor layer of height $h \equiv 1$ has no contribution to the energy $\overline{E}$, we shift h by -1 and consider the problem

$$\text{Minimize} \quad \int \tfrac{1}{2} |\nabla h|^2 \, dx + \; \mathrm{vol}\,(\{h > 0\}) \;\; \text{subject to} \;\; \int h \, dx = V. \tag{A.3}$$

For convenience, we keep the notation h for the shifted film height.

Proposition 3. *Let $V \ge 0$. Then there exists a constant $H > 0$ depending on V such that*

$$\bar{h}(x) \;=\; -\tfrac{1}{2H}|x|^2 + H \qquad \text{on } B(0, \sqrt{2}H), \tag{A.4}$$

is the unique (up to translations) minimizer of problem (A.3).

Proof. We proceed in three steps:

(1) Any minimizer $\bar{h}$ of (A.3) is radially symmetric and monotonically decreasing.
(2) Any minimizer $\bar{h}$ satisfies
$$-\Delta\bar{h} \;=\; \text{const} \qquad \text{in } \{\bar{h}>0\}. \tag{A.5}$$
(3) A unique (up to translations) minimizer $\bar{h}$ exists and satisfies
$$\tfrac{1}{2}|\nabla\bar{h}|^2 \;=\; 1 \qquad \text{on } \partial\{\bar{h}>0\}. \tag{A.6}$$

Argument for (1): The proof is based on the symmetric decreasing rearrangement $h^{\#}$ of the function h. It is well known ([13, Lemma 7.17]) that
$$\int |\nabla h^{\#}|^2\,dx \;\le\; \int |\nabla h|^2\,dx$$
with equality if and only if h is radially symmetric and monotone decreasing. Furthermore, the second contribution to the energy is conserved:
$$\text{vol}\,(\{h^{\#}>0\}) \;=\; \text{vol}\,(\{h>0\}).$$

Argument for (2): The first variation of $\overline{E}$ yields
$$\int (-\Delta h)\,\delta h\,dx \;=\; 0$$
for all variation δh with
$$\int \delta h\,dx = 0 \quad \text{ and } \quad \text{supp}\,\delta h \subset \{h>0\}.$$
Hence we obtain (A.5).

Argument for (3): From (1) and (2), we deduce that any minimizer centered at the origin must be of the form
$$h(x) = -A|x|^2 + H \qquad \text{on } B(0,\sqrt{H/A}). \tag{A.7}$$
Note that the family of candidates is invariant under the volume-conserving homothetic variation:
$$h_\lambda(x) \;=\; \lambda^{-n} h\left(\frac{x}{\lambda}\right).$$
Then the first variation of $\overline{E}$ in λ at $\lambda=1$ yields that at a critical point $\bar{h}$
$$(n+2)\int \tfrac{1}{2}|\nabla\bar{h}|^2\,dx \;=\; n\ \text{vol}\,(\{\bar{h}>0\}). \tag{A.8}$$
Note that the critical point is in fact a minimum since the function
$$\lambda \;\mapsto\; E(h_\lambda) = \lambda^{-(n+2)}\int \tfrac{1}{2}|\nabla\bar{h}|^2\,dx + \lambda^n\ \text{vol}\,(\{\bar{h}>0\}).$$
is convex. We compute
$$\int_{\{\bar{h}>0\}} \tfrac{1}{2}|\nabla\bar{h}|^2\,dx = \tfrac{2}{n+2}\omega_n A^2(\sqrt{H/A})^{n+2}$$
and
$$\text{vol}\,(\{\bar{h}>0\}) \;=\; \tfrac{1}{n}\omega_n(\sqrt{H/A})^n,$$

where ω_n denotes the $(n-1)$-dimensional measure of $\mathbb{S}^{n-1}$. Thus we obtain from (A.8) that for the minimizer

$$2AH = 1. \tag{A.9}$$

Hence at $\partial\{\bar{h} > 0\}$ where $|x|^2 = H/A$,

$$|\nabla \bar{h}|^2 \;=\; 2$$

which proves (3). Furthermore, we obtain from (A.7) and (A.9) that

$$\bar{h}(x) \;=\; -\tfrac{1}{2H}|x|^2 + H \qquad \text{on } B(0, \sqrt{2}H).$$

□

Remark 5. *Proposition 3 reveals the scaling* (1.10)

$$H \;\sim\; R,$$

since the radius of the droplet is given by $\sqrt{2}H$.

Appendix B. The gradient flow structure

In this section, we specify in which sense the evolution (1.4) is a gradient flow of E defined in (1.2). This heuristic section serves purely as a motivation which guides our analysis. The rigorous result is independent of this section.

The mathematical structure required for a gradient flow

$$\partial_t h \;=\; -\mathrm{grad} E(h). \tag{B.1}$$

is determined by a smooth function $\mathcal{M} \ni h \mapsto E(h)$ on a Riemannian manifold $(\mathcal{M}, g)$. A trajectory $[0,\infty) \ni t \mapsto h(t) \in \mathcal{M}$ of (B.1) is characterized by the fact that for any tangent vector field $[0,\infty) \ni t \mapsto \delta h(t) \in T_{h(t)}\mathcal{M}$, one has

$$g_{h(t)}\left(\partial_t h(t), \delta h(t)\right) + \left\langle \mathrm{diffE}_{h(t)}, \delta h(t) \right\rangle \;=\; 0 \quad \text{for all } t \geqslant 0. \tag{B.2}$$

In our case $\mathcal{M}$ corresponds to the space of all possible film heights which take the overall mass constraint into account:

$$\mathcal{M} \;= \left\{ h \geq 0 \;\middle|\; \int h(x)\, dx = \int 3\, dx \quad \right\}.$$

The metric tensor encodes the limiting dissipation mechanism by (viscous) friction. Given the continuity equation $\partial_t h + \nabla \cdot (h\, u) = 0$ for the film height $h \geq 0$ by a (vertically averaged horizontal) velocity field $u \in \mathbb{R}^n$, the rate of energy dissipation by friction is given by $\int h\, |u|^2\, dx$ in the case of Darcy-type friction. (It would be $\int \frac{1}{h}|u|^2\, dx$ for Stokes friction with no-slip boundary conditions.) The (quadratic part of) the metric tensor is given by

$$g_h(\delta h, \delta h) \;=\; \inf_u \left\{ \int h|u|^2\, dx \;\middle|\; \delta h + \nabla \cdot (hu) = 0 \right\}. \tag{B.3}$$

For the sake of simplicity, we do not state the boundary conditions like $\nu \cdot u = 0$ on ∂Q. The squared size, $g_h(\delta h, \delta h)$, of an infinitesimal perturbation δh is the minimal rate of energy dissipation by friction which is necessary to generate δh.

Writing down the Euler–Lagrange equation for (B.3) yields the following representation in terms of the velocity potential φ:

$$g_h(\delta h, \delta h) = \int h|\nabla\varphi|^2 \, dx \qquad \text{where} \quad \delta h + \nabla \cdot (h\nabla\varphi) = 0.$$

By polarization, this yields

$$g_h(\delta h_1, \delta h_2) \;=\; \int h \, \nabla\varphi_1 \cdot \nabla\varphi_2 \, dx, \tag{B.4}$$

where the functions φ_i are defined by

$$\delta h_i + \nabla \cdot (h\nabla\varphi_i) = 0.$$

It is easy to check that indeed (1.4) is the gradient flow of (1.2) in the sense of (B.2) with respect to the metric tensor (B.4) defined on $\mathcal{M}$.

Any Riemannian manifold $(\mathcal{M}, g)$ is endowed with a natural distance function d between two points h_0 and h_1 by means of minimizing the action of curves from h_0 to h_1. In view of the definition of the metric tensor (B.3), d turns into

$$d(h_0, h_1)^2 \;=\; \inf_{(h,u)} \left\{ \int_0^1 \int h|u|^2 \, dxds \;\middle|\; \partial_s h + \nabla \cdot (hu) = 0, \left\{ \begin{array}{l} h(0,\cdot) = h_0 \\ h(1,\cdot) = h_1 \end{array} \right\} \right\}.$$

It is shown in [23] that d in fact coincides with the Wasserstein distance $\mathcal{W}$ defined above in (1.5).

Acknowledgements. Felix Otto acknowledges partial support by the Sonderforschungsbereich 611 *Singular phenomena and scaling in mathematical models* at Bonn University. Tobias Rump acknowledges support by the Sonderforschungsbereich 611. Dejan Slepčev acknowledges support by NSF grant DMS-0244498 and ONR grant N000140410078. He would also like to thank University of Bonn for hospitality and Sonderforschungsbereich 611 for supporting his visits.

The authors thank Patrick Penzler and Maria Reznikoff for fruitful discussions.

References

[1] J. Becker, G. Grün, R. Seeman, H. Mantz, K. Jacobs, K. R. Mecke, and R. Blossey. Complex dewetting scenarios captured by thin-film models. *Nature Materials*, 2(1):59–63, 2003.

[2] A. L. Bertozzi, G. Grün, and T. P. Witelski. Dewetting films: bifurcations and concentrations. *Nonlinearity*, 14(6):1569–1592, 2001.

[3] S. Conti, B. Niethammer, and F. Otto. Coarsening rates in off-critical mixtures. *to appear in SIAM J. Math. Anal.*, 2005.

[4] S. Dai and R. L. Pego. Universal bounds on coarsening rates for mean-field models of phase transition. October 2004.

[5] S. Dai and R. L. Pego. An upper bound on the coarsening rate for mushy zones in a phase-field model. *Interfaces Free Bound.*, 7(2):187–197, 2005.

[6] K. B. Glasner and T. P. Witelski. Coarsening dynamics of dewetting films. *Phys. Rev. E*, 67(1):016302, 2003.

[7] K. B. Glasner and T. P. Witelski. Collision vs. collapse of droplets in coarsening of dewetting thin films. Preprint, April 2004.

[8] S. Herminghaus, K. Jacobs, K. Mecke, J. Bischof, A. Fery, M. Ibn-Elhaj, and S. Schlagowski. Spinodal dewetting in liquid cristal and liquid metal films. *Science*, 282(10):916–919, 1998.
[9] J. N. Israelachvili. *Intermolecular and Surface Forces*. Academic Press, New York, second edition, 1992.
[10] R. V. Kohn and F. Otto. Upper bounds on coarsening rates. *Comm. Math. Phys.*, 229(3):375–395, 2002.
[11] R. V. Kohn and X. Yan. Upper bound on the coarsening rate for an epitaxial growth model. *Comm. Pure Appl. Math.*, 56(11):1549–1564, 2003.
[12] R. V. Kohn and X. Yan. Coarsening rates for models of multicomponent phase separation. *Interfaces Free Bound.*, 6(1):135–149, 2004.
[13] E. H. Lieb and M. Loss. *Analysis*, volume 14 of *Graduate Studies in Mathematics*. American Mathematical Society, Providence, RI, second edition, 2001.
[14] R. Limary and P. F. Green. Late-stage coarsening of an unstable structured liquid film. *Phys. Rev. E*, 66(2), 2002.
[15] R. Limary and P. F. Green. Dynamics of droplets on the surface of a structured fluid film: Late-stage coarsening. *Langmuir*, 19(6):2419–2424, 2003.
[16] A. Münch. Dewetting rates of thin liquid films. *J. Phys. condensed Matter*, 17(9):S309–S318, 2005.
[17] A. Münch and B. Wagner. Contact-line instability of dewetting thin films. WIAS Preprint No. 924, 2004.
[18] B. Niethammer and F. Otto. Domain coarsening in thin films. *Comm. Pure Appl. Math.*, 54(3):361–384, 2001.
[19] A. Oron and S. G. Bankoff. Dewetting of a heated surface by an evaporating liquid film under conjoining/disjoining pressures. *J. Colloid Interface Sci.*, 218(1):152–166, 1999.
[20] A. Oron, S. H. Davis, and S. G. Bankoff. Long-scale evolution of thin liquid films. *Rev. Mod. Phys.*, 69(3):931–980, 1997.
[21] F. Otto, P. Penzler, and T. Rump. Discretisation and numerical tests of a diffuse–interface model with Ehrlich–Schwoebel barrier. In *Multiscale Modeling in Epitaxial Growth*, volume 149 of *International Series of Numerical Mathematics*, pages 127–158. Birkhaeuser, 2005.
[22] F. Otto and C. Villani. Generalization of an inequality by Talagrand and links with the logarithmic Sobolev inequality. *J. Funct. Anal.*, 173(2):361–400, 2000.
[23] F. Otto and M. Westdickenberg. Eulerian calculus for the contraction in the Wasserstein distance. accepted for *SIAM J. Math. Anal.*
[24] L. M. Pismen. Spinodal dewetting in volatile liquid film. *Phys. Rev. E*, 70:051604, 2004.
[25] L. M. Pismen and Y. Pomeau. Mobility and interactions of weakly nonwetting droplets. *Phys. Fluids*, 16(7):2604–2612, 2004.
[26] G. Reiter. Dewetting of thin polymer films. *Phys. Rev. Lett.*, 68(1):75–78, 1992.
[27] G. Reiter and R. Khanna. Kinetics of autophobic dewetting of polymer films. *Langmuir*, 16:6351–6357, 2000.
[28] R. Seeman, S. Herminghaus, and K. Jacobs. Gaining control of pattern formation of dewetting liquid films. *J. Phys. Condensed Matter*, 13:4925–4938, 2001.
[29] A. Sharma and R. Khanna. Pattern formation in unstable thin liquid films. *Phys. Rev. Lett.*, 81:3463–3466, 1998.
[30] U. Thiele, M. G. Velarde, and K. Neuffer. Dewetting: film rupture by nucleation in the spinodal regime. *Phys. Rev. Lett.*, 87(1):4, 2001.
[31] F. Vandenbrouck, M. P. Valignat, and A. M. Cazabat. Thin nematic films: metastability and spinodal dewetting. *Phys. Rev. Lett.*, 82:2693–2696, 1999.
[32] C. Villani. *Topics in optimal transportation*, volume 58 of *Graduate Studies in Mathematics*. American Mathematical Society, Providence, RI, 2003.
[33] R. Xie, A. Karim, J. F. Douglas, C. C. Han, and R. A. Weiss. Spinodal dewetting of thin polymer films. *Phys. Rev. Lett.*, 81(6):1251–1254, 1998.

Felix Otto, Institute for Applied Mathematics, University of Bonn, Wegelerstrasse 10, D–53115 Bonn, Germany
E-mail address: otto@iam.uni-bonn.de

Tobias Rump, Institute for Applied Mathematics, University of Bonn, Wegelerstrasse 10, D–53115 Bonn, Germany
E-mail address: rump@iam.uni-bonn.de

Dejan Slepčev, Mathematics Department, UCLA, Box 951555, Los Angeles, CA 90095, U.S.A.
E-mail address: slepcev@math.ucla.edu